Microelectronic Engineering 237 (2021) 111478

Contents lists available at ScienceDirect

Microelectronic Engineering

journal homepage: www.elsevier.com/locate/mee

Research paper

Soft and flexible gold microelectrodes by supersonic cluster beam deposition and femtosecond laser processing

Tali Dotan [a,b,*], Yuval Berg [a,c], Lorenzo Migliorini [d], Sara Moon Villa [d], Tommaso Santaniello [d], Paolo Milani [d], Yosi Shacham-Diamand [a,b]

[a] Department of Physical Electronics, School of Electrical Engineering, Faculty of Engineering, Tel- Aviv University, Ramat Aviv, 69978, Israel
[b] Department of Materials Science and Engineering, Faculty of Engineering, Tel- Aviv University, Ramat Aviv, 69978, Israel
[c] Additive Manufacturing Group, Orbotech Ltd PO Box 215, Yavne 81101, Israel
[d] CIMAINA and Physics Department, Università degli Studi di Milano, Via Celoria 16, I-20133, Milano, Italy

ARTICLE INFO

Keywords:
Microelectrodes
Micropatterning
Flexible electronics
Supersonic cluster beam deposition
Femtosecond lasers
Nanocomposite films

ABSTRACT

Soft and flexible microelectrodes are fabricated and patterned in a novel approach integrating supersonic cluster beam deposition (SCBD) of gold nanoparticles onto Polydimethylsiloxane (PDMS) followed by femtosecond (fs) laser processing. SCBD of gold nanoparticles in PDMS forms a nanocomposite film with mechanical properties similar to those of the elastomeric substrate. Electrically neutral metallic nanoparticles penetrate the polymeric matrix and distribute randomly up to a depth of a few hundred nanometers forming a path of ohmic conduction. High resolution patterning on soft substrates is a major challenge that was overcome by femtosecond laser ablation of micrometer lines with relatively very little thermal damage. Microelectrodes were fabricated with a width down to 3 μm. The printed metal line sheet resistance was 480 Ohm/square for the 100 nm thick film and 210 Ohm/square for the 200 nm thick film. The calculated average film specific resistivity was found to be 2.5–2.6mΩ·cm. It is ~3 orders of magnitude higher than that of physical vapor deposited gold; therefore, it is not suitable for high current interconnects but sufficient for low-current signal transmission such as for electrical and electrochemical biosensors.

1. Introduction

Soft and flexible electronics have been under intense research and development for various applications, e.g. wearables and bio-implants. Traditional electrodes are patterned on rigid substrates such as silicon or glass or on a flexible substrate such as polyimide. Those materials have mechanical characteristics that are very different than those of biologic surfaces. Therefore, placing electrodes on biological entities results in incomplete or ineffective contact deteriorating the signal and introducing noise. The signal deterioration can be in the form of attenuation and instabilities due to the relative movement of the electrodes and the biological entity, i.e. skin, leaf, etc. A possible solution to those problems is the use of soft and flexible electrodes mimicking the mechanical compliance of the biologic tissue. Such soft and flexible electrodes have already been applied in various applications using technologies such as neuroelectrodes [1], skin prosthesis [2], skin patchable electrodes [3,4] and electrochemical analysis by lab-on-a-chip on plastic, paper and textiles [5].

There are few candidates for soft and flexible electrodes, such as elastomeric polymers. Polydimethylsiloxane (PDMS) is the most obvious candidate today. PDMS is commonly used for biomolecular interfaces due to its elasticity, transparency, stability, biocompatibility, and its unique characteristics that allow surface functionalization, e.g. specifically modifying a material's surface functionality [6–8]. Gold electrodes on PDMS have been widely demonstrated in previous studies such as [1,9–19]. There are two main challenges in the integration of rigid metal film on the elastomeric substrate.

a. Mechanical incompatibility of the two materials. The difference of the Young modulus [20] and the coefficient of thermal expansion (CTE) [21] between the two materials cause mud- like cracking of the surface.
b. Processing incompatibility - Micro-patterning metallic layer on polymers.

* Corresponding author at: Department of Physical Electronics, School of Electrical Engineering, Faculty of Engineering, Tel- Aviv University, Ramat Aviv, 69978, Israel
E-mail address: talidot@gmail.com (T. Dotan).

https://doi.org/10.1016/j.mee.2020.111478
Received 15 July 2020; Received in revised form 3 November 2020; Accepted 7 November 2020
Available online 12 November 2020
0167-9317/© 2020 Published by Elsevier B.V.

The mechanical problems appear in the form of cracking effects that may frequently occur in nanometer-thick metal films that are deposited, typically by physical vapor deposition (PVD) onto polydimethylsiloxane (PDMS) substrates. It was suggested by Baëtens et al. [22] that prior to the metal deposition, a thin, brittle silica-like crust is formed on the PDMS surface due to oxygen plasma. The deposition of a thin metal film subsequently generates cracks on the surface due to residual tensile stress with density dependent on the film's thickness. Additional studies have addressed this phenomenon, often referred to as "dry mud" islands [23]. Akogwu et al. have suggested that the cracks are formed by residual stress arising from the CTE differences between the elastomeric substrate and the gold thin film [21]. Seghir and Arscott proposed that the cracking of the silica-like crust and the metal film occurs if the residual tensile stresses are greater than the ultimate tensile strengths of layers [20]. In not-yet published work by Turjeman et al. [24], our group has developed a process to fabricate defect and stress-free metal thin film on elastomers through modelling their mechanical behavior. A few researchers have reported creating a percolating network that allows electrical continuity but suffer from high resistivity [21,23,25].

In this work, the electrodes on the elastomer were metallized by Supersonic Cluster Beam deposition (SCBD) of gold nanoparticles. This is a manufacturing technique relying on the use of supersonically accelerated beams of neutral metal clusters that can be directed onto a polymeric target to generate thin cluster-assembled metal layers physically interpenetrating with the polymer [26]. The process takes place at room temperature and involves low kinetic energies of the nanoparticles, avoiding thermal damage or chemical modification of the polymeric matrix under impact [14,27]. Using this method, the mechanical properties of the nanocomposite can be maintained close to that of the bare elastomer for significant metal volume concentrations [14]. Nanocomposite films with NP density above the critical value show electrical transport properties which are typical of thin metallic films [28].

The second integration challenge that needed to be resolved was gold line microscale patterning on the PDMS. Previous works on SCBD metallization over PDMS used stencil (shadow) masks for patterning where the acquired feature size was in the range of tens of microns [29]. The use of stencil masks has both resolution limits and also field size limits depending on the shadow mask span. Other candidates for printing small size features are transfer printing [19,30], laser induced forward transfer [31–34] and photolithography [1,10,18]. The latter is commonly used in thin film technologies on rigid and flexible substrates. However, photolithography on elastomers is a challenge and it is usually done when there is a rigid substrate under the soft material. Additionally, the large coefficient of thermal expansion and the swelling process of elastomers limit the minimum patterned feature size to about 100 μm [13] for conventional lithography.

In this work, femtosecond (fs) laser ablation was used for patterning the PDMS/Au nanocomposite film. Ultrashort laser ablation is unique in its capabilities of high spatial precision, minimal collateral thermal damage, high material removal rate, selective ablation of thin layers and the capability of processing a large range of materials. The ultrashort time of excitation allows the separation of the involved processes as excitation, melting, and material removal [35]. Ultrashort pulsed laser ablation stands out in the important role played by thermal effects. These include not only vaporization from the extreme outer surface and boiling from an extended near-surface region, but also phase explosion.

Thin film ablation on both planar and non-planar surfaces has been previously demonstrated [36–39]. The control parameters for providing ablation selectivity (i.e. complete removal of the thin film and leaving the substrate intact) are the laser fluence and scanning velocity (correlating to pulse overlap). The selectivity depends on the optical properties of both the substrate and the thin film.

The fabrication of soft and flexible electrodes with sub10 micrometer resolution faces severe problems emerging from both the materials' mechanical and surface properties, compatibility with conducting materials and also very often due to non-planar topography. The objective of this work was to develop a full integrated technology incorporating the metallization and patterning to achieve microelectrodes on flexible and soft polymers for various applications, e.g. electrochemical and electrical bio sensors, chemical sensors.

2. Methods and experimental details

The first step of the fabrication process is the PDMS substrate preparation. The pre-polymer gel and the cross linker (Sylgard® 184, Dow Inc.) are mixed at a 20:1 (*w*/w) ratio. The mixture is poured into a metal mold, and degassed thoroughly. The PDMS is cured in a pre-heated oven at 125 °C for 75 min and cooled down at room temperature. A 500 μm film was obtained. The PDMS substrate was mounted onto a sample holder and inserted into a vacuum chamber in the SCBD system.

The SCBD system consists of a pulsed micro-plasma cluster source (PMCS), an aerodynamic focuser, an expansion chamber, an implantation chamber and system of moving sample holders [40]. An Argon plasma is formed by high voltage discharge (750 V) and erodes a golden rod target placed in the PMCS. Sputtered gold atoms thermalize with argon and aggregate, creating a mixture of clusters and inert gas which exit the PMCS through a nozzle as a supersonic seeded beam of electrically neutral clusters. The beam passes through aerodynamic focuser where the nanoparticles are focused. It then expands at the expansion chamber where high vacuum is kept (10^{-7} Torr) and moves through the skimmer to the implantation chamber. The metal nanoparticles impact and penetrate the polymeric matrix with a soft implantation, without inducing any chemical or physical alteration due to their low kinetic energy (~0.5 eV/atom). During the deposition, the film thickness was monitored in-situ by alternatively directing the beam towards the PDMS samples and a quartz microbalance. The measured deposited mass was used to calculate the equivalent thickness t_{eq}, defined as the thickness of the film that a certain mass of clusters would form on a smooth, rigid surface of a hard substrate (e.g. silicon). The film resistivity was measured in- situ as well during the deposition process, to make sure that the deposited layer has a gold concentration above the percolation threshold. In this work, the deposited films were characterized by an equivalent thickness of 50, 100, 150, and 200 nm and a surface area of about 2 cm^2.

The patterning of the microelectrodes was done using Amplitude Systems Tangerine HP ultrashort laser ablation in atmospheric pressure. The laser wavelength was 343 nm, the pulse duration was 270 fs and the repetition rate was 12.5 kHz, maintained by pulse picking the fundamental 175 kHz repetition rate. The pulse fluence used was within the range of 0.3–1.14 μJ and was controlled by an internal acousto-optic modulator. A fast-galvanometric scanner followed by an F-theta lens (focal length = 100 mm) scans the linearly-polarized, 10 μm Gaussian laser spot diameter on the surface. The scanning velocity range was within the range of 12.5 mm/s to 250 mm/s.

Electrode lines were patterned using laser ablation of SCBD PDMS/AuNP films. The metal is ablated with equal-spaced and 50% overlap trenches so that it will act as an insulator while the electrodes remain unablated. The electrode length is 2 mm and their width values were 200 μm, 160 μm, 90 μm, 30 μm and 23 μm, 13 μm, and 3 μm.

The resistivity was measured from the current vs. voltage characteristics in a voltage sweep mode between 0 and 100 mV. The electrical characterization was carried out using a Keithley 2450 Source-Monitor-Unit (SMU) with wide and blunt end tips connected to the measurement system to prevent the penetration of the tips into the soft substrate.

HRSEM images were taken with tungsten deposition using 5 keV acceleration voltage and 0.4 nA beam current. The FIB cross section was processed with 30 V and 0.79 nA gallium dual beam system.

3. Results and discussion

3.1. Surface morphology

Fig. 1 shows images of the films which were fabricated by SCBD. Subsets (a) and (c) depict SEM cross sections of a PDMS substrate with 50 nm and 200 nm equivalent thickness, respectively and subsets (b) and (d), show SEM tops views of the surface morphology of 50 nm and 200 nm equivalent thickness, respectively. It can be seen that the gold nanoparticles create a fully covered layer and penetrate the PDMS surface to form a PDMS/ Au nanocomposite film. The film is comprised of 5–15 nm particles which maintain their shape in a randomly distributed structure.

Table 1 shows the parameters of the nanocomposte film. The actual measured thickness of the different films is presented against their equivalent thicknesses (t_{eq})- the thickness of a reference film deposited on a quartz microbalance using the same process conditions during the deposition. The equivalent thickness is measured on a hard substrate where the layer is deposited on top of the substrate and in the described process has a 50% gold density, or 9.66 g/cm^3. It can be seen that the density of the film increases with its thickness, and is in the range of 23–30% of the volume which correlates to 4.4–5.8 g/cm^3. The relatively low concentration of the gold nanoparticles in the PDMS matrix provides unique properties combining the matrix mechanical properties with the gold conductivity. The standard deviation of the measured thickness decreases with increasing film thickness, meaning that the uniformity of the film increases with its thickness (see Table 1).

As shown in Fig. 2, the actual thickness of the film is significantly larger than that of the equivalent thickness. The relation between the actual thickness and the equivalent thickness can be fitted to the following equation:

$$t_{actual} = k_1 \cdot t_{eq}^{\,k_2}. \quad (1)$$

where $k_1 = 6.048$ and $k_2 = 0.759$ ($r^2 = 0.987$) (where both are in nm).

The composite material consists of the PDMS and the gold clusters. The initial pre- implantation PDMS has a low young modulus (of about 1.32–2.97 MPa [41]) and easily deforms as a response to an applied strain. During the gold cluster implantation, the composite material includes more than 20% gold in volume and 4 g/cm^3 in mass. The newly implanted clusters apply a force on the film including on the gold clusters in the film and push them further in the depth of the film. We assume that despite the fact that the gold percentage inside the composite film is below 50%, the two composites of the film form a well-organized, compact structure that does not allow further penetration of more clusters.

The layers' sheet resistance was measured on site. We characterized films with equivalent thickness in the range of 50-200 nm. The sheet resistance of the 50 nm equivalent thickness samples was very high while the rest were significantly low. Regarding the thicker gold samples, their sheet resistance allowed calculating the specific resistivity that decreased with increasing thickness. This indicates that the higher the gold concentration in the film is, the more conductive the

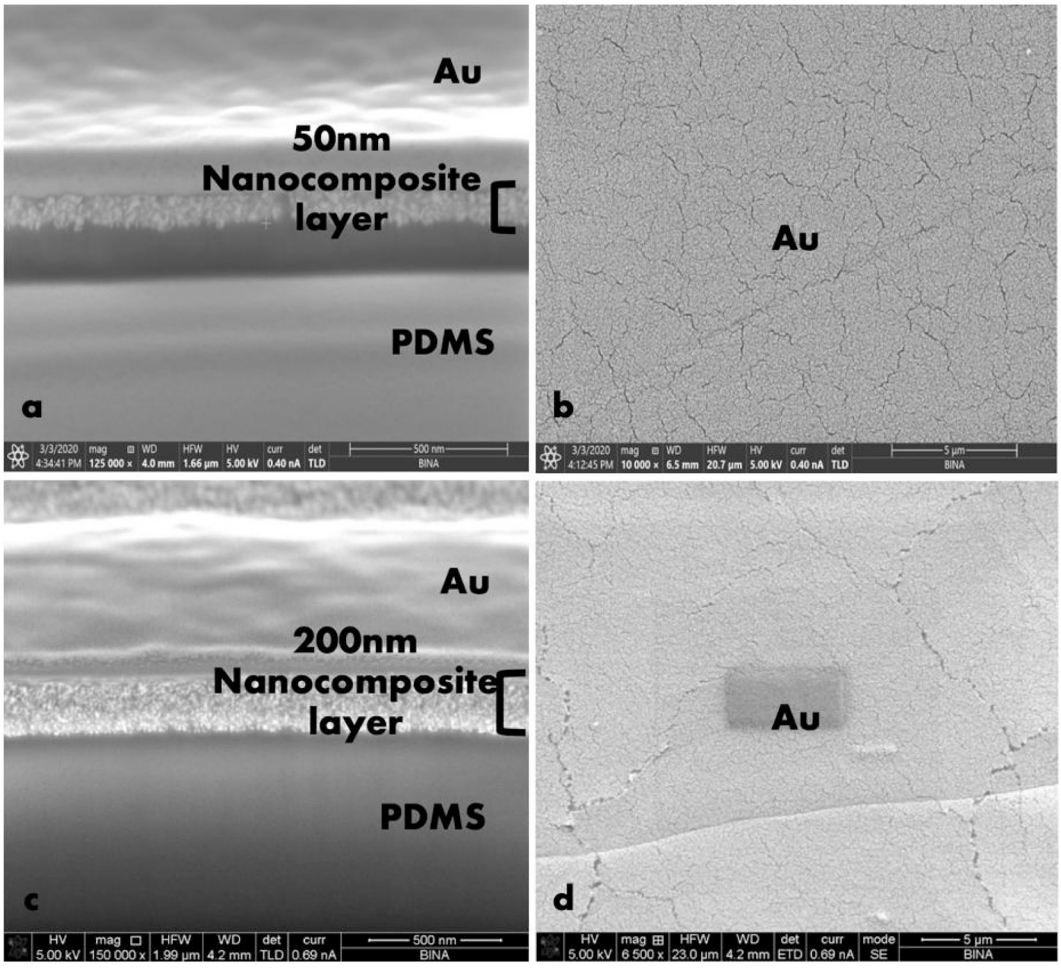


Fig. 1. SEM images of gold NP/ PDMS nanocomposite films fabricated by supersonic cluster beam deposition (SCBD). (a) and (c) FIB cross sections of 50 nm and 200 nm equivalent thickness respectively. (b) and (d) microcracks on gold surface of 50 nm and 200 nm equivalent thickness respectively. (For interpretation of the references to colour in this figure legend, the reader is referred to the web version of this article.)

Table 1
SCBD Gold/ PDMS film parameters.

Equivalent thickness [nm]	Actual thickness [nm]	Standard deviation [nm]	Percent gold [%(v/v)]	Gold density in film [g/cm^3]	Thin Film Sheet resistance [Ω/sq]	Fabricated Line Sheet resistance [Ω/sq]	Resistivity [Ω · cm]
50	114.1	19.9	21.9	4.23	–		
100	213.4	16.7	23.4	4.53	480	123.3	$2.63 \cdot 10^{-3}$
150	265.7	11.7	28.2	5.45	290		
200	330.3	4.3	30.3	5.85	210	75.1	$2.48 \cdot 10^{-3}$

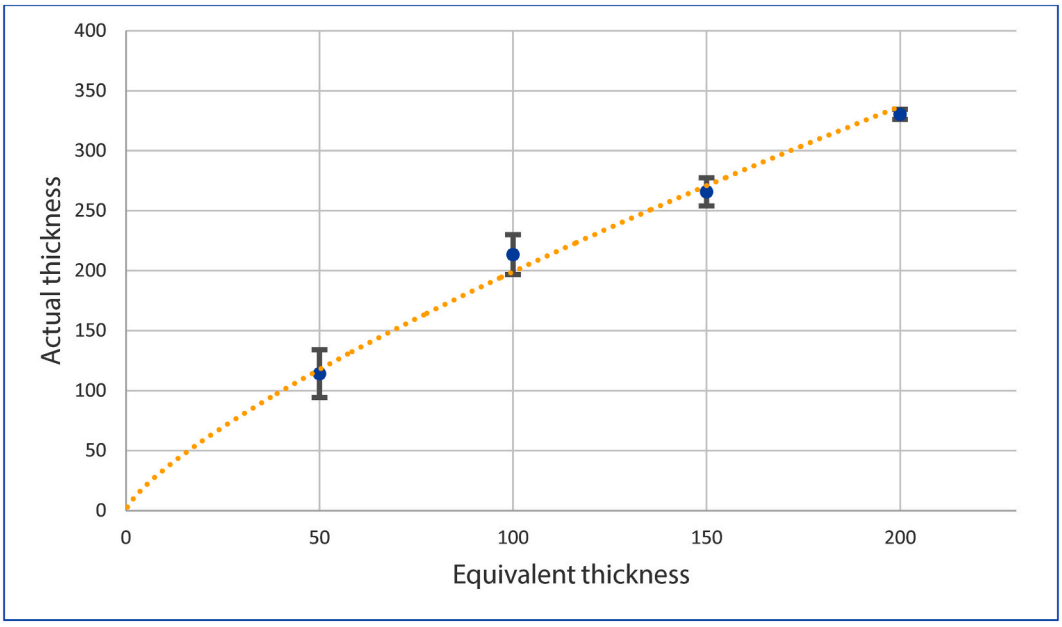


Fig. 2. Measured thickness (actual thickness) vs. the equivalent thickness. Dots represent the analyzed films and the dashed line is the best fitting.

microelectrode is.

The SEM images (see Figs. 1(b) and 1(d)) reveal microcracks in all of the deposited films, however their magnitudes differ from sample to sample. The 50 nm equivalent thickness film depicts “dry mud” islands of 1-5 μm with cracks of ~ a few tens of nm while the 200 nm equivalent thickness film had 20-40 μm islands and cracks above 100 nm thickness. This result is compatible with other studies done on conventional gold films where the increasing film thickness is associated with an increase in film grain size [21].

Unlike gold films deposited by conventional methods (e.g. e- beam

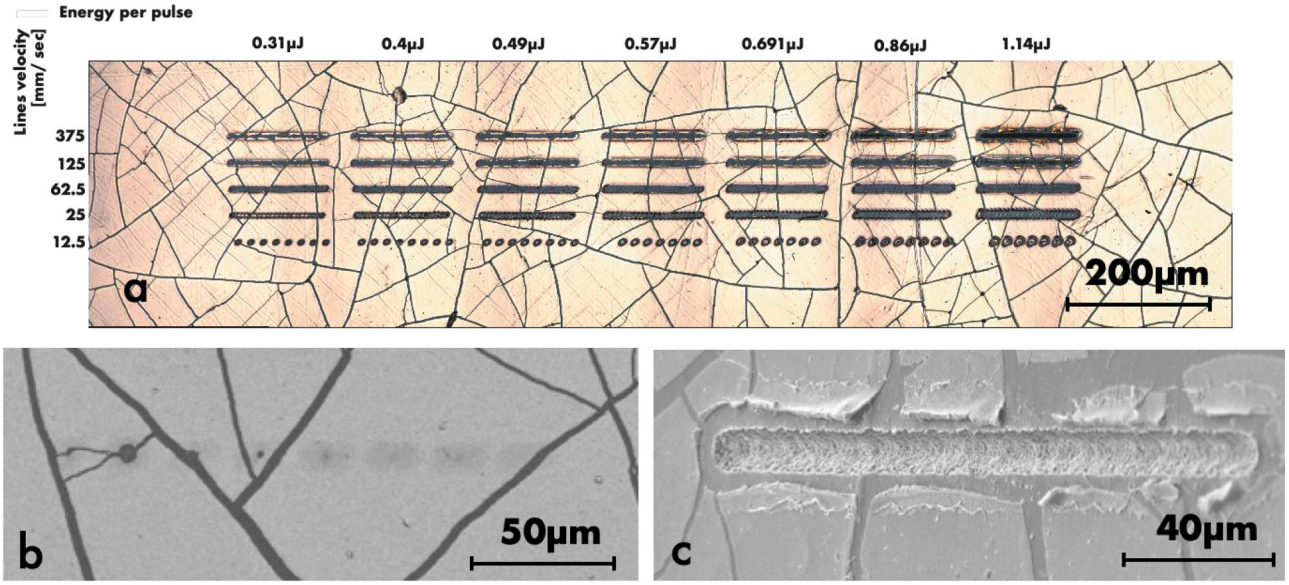


Fig. 3. Femtosecond laser ablated lines on nanocomposite films. (a) Optical imaging of matrix-line velocity [mm/s] vs. laser energy patterning [μJ]. (b) and (c) SEM imaging of zoomed patterning tests (a) 12.5 mm/s, 0.3 μJ (b) 375 mm/s, 1.14 μJ.

evaporation, sputtering etc.), the observed cracks are present only on the surface layer of the composite film. In the depth of the film, the cracks are very narrow and keep a close enough proximity between the particles to allow a conductive path.

3.2. Femtosecond laser patterning of AuNP film

The process window was optimized with a series of femtosecond laser procedures. Spot size, pulse temporal width, and Pulse repetition rate (PRR) were set to fixed values of ~10 μm, 270 fs and 12.5 kHz accordingly, while laser fluence and scanning velocities (pulse to pulse overlap) were varied. Fig. 3 depicts a typical matrix of such procedure.

The processed material has a non-uniform surface composed of randomly distributed gold nanoparticles in a PDMS matrix. The microprocessing opts to ablate and remove the gold aggregates from inside the film and have minimal effect on the polymer. The two materials have very dissimilar optical properties as the ablation threshold for gold surfaces were previously reported as 210–244 mJ/cm^2 [42,43] and the PDMS ablation threshold is 4.6 J/cm^2 [44]. A large process window is suggested in the range higher than the gold ablation threshold and lower than that of PDMS. A sweep of fluences in the defined region was carried out to find an optimal point, while scanning velocity (pulse to pulse overlap) was set from separated pulses to high overlap (>90%), where fabrication of good line roughness was targeted.

Two different phenomena can be observed in the two ends of the span, as shown in Fig. 3(b) and 3(c). In the low fluence regime (Fig. 3 (b)), single shots (bottom row lines) do not cause complete gold removal, since the fluence is not sufficient to fully-ablate the gold from the composite material. It can be suggested that gold nanoparticles in a polymeric matrix require higher fluence than standard gold film and also from gold NP induced film [45]. The continuous lines have lower scan velocity, meaning that the high overlap of the pulses results in full removal of the gold, as studied in a previous work [46].

As expected, for high fluence and low velocity, the laser processing induces PDMS ablation (Fig. 3(c)). In these process conditions, the gold is fully ablated but there is also significant surface damage. Based on the above observations, the process was tuned to a fluence of 400 mJ/cm^2 and scan speed of 45 mm/s, where clean patterning of low roughness lines was achieved.

3.3. Electrical characterization

Fig. 4 shows the measured sheet resistance multiplied by the actual thickness of the film ($R_s \cdot t_{actual}$) as a function of the film's actual thickness. The actual thickness is calculated by using the experimental dependence which had been found by fitting the measured thickness with its theoretical thickness as presented in Fig. 2 (Eq. 1). By definition, the measured sheet resistance can be expressed as $R_s = \rho \frac{l}{w \cdot t_{actual}}$. By rearrangement of the parameters we get that $R(t) \cdot t_{actual} = \rho(t) \frac{l}{w}$: the dependence of the function on the density of the film and its geometry. Since the length and width of the measurement sample don't change as the thickness of the deposited film grows, the trend is proportional to the resistivity of the film at each point. The behavior of resistivity can be separated in the two regimes. The pure PDMS has a very high resistivity of $4 \cdot 10^{15}$ Ω·cm. The implanted gold clusters provide electric conductance due to two different mechanisms- electrons tunneling effects and physical contact between conductor clusters (ohmic conductance). At low thickness, the "tunneling controlled regime", there is an exponential decay that can be attributed to tunneling effects. According to quantum mechanics tunneling theory, electrons in dispersed conducting particles in an insulator matrix can move between one conducting particle to another through tunneling. As shown by Simmons [47], the tunneling resistivity depends exponentially on the tunneling distance, or as presented in our experiment, it depends exponentially on the concentration of implanted conducting clusters in the insulating matrix. For a very small concentration, the distance between the adjacent clusters is higher than the electron- tunneling distance and no current is measured. At thicknesses higher than 200 nm, there is an "ohmic conduction regime" where a percolation network is formed. At these thicknesses the resistivity reaches a constant value, not dependent on the thickness or the density of the film. The electron passage is through contact between gold clusters, so that when a sufficient amount of connections is formed, the addition of gold does not change the conductance of the film.

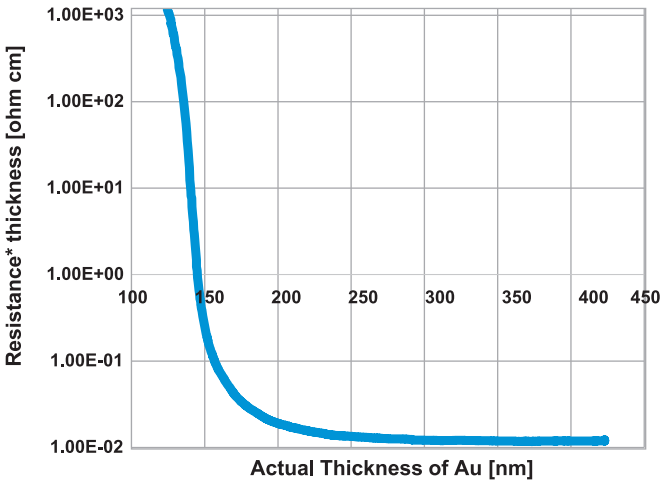


Fig. 4. Percolation curve. Presentation of the in-situ sheet resistance of gold NP/ PDMS nanocomposite film multiplied by the calculated actual thickness [Ωcm] vs the calculated actual thickness [nm].

Fig. 5 represents SEM and optical imaging of microelectrodes with varying line-width between 3 μm and 200 μm and 2 mm length. The microelectrodes were patterned using fs laser ablation process as described above with 0.3 μJ/pulse and pattern velocity of 45 mm/s. Ablation in a constant velocity was used in 50% overlap equally spaced lines to remove the conducting layer from the background, leaving a conducting layer only on the electrodes themselves.

The array of microelectrodes was tested, patterned on 75 nm t_{eq} film. All of the electrodes were conductive including 3 μm wide electrode. The measured sheet resistance 2.1–2.6kΩ/sqr.

Fig. 6 depicts the relation between 1/R to the electrode's width where R is the measured resistance of the electrode. The graph presents two trends of 100 nm and 200 nm t_{eq} films, where both have a linear relation with an ascending slope between 0.0015 and 0.02 cm. Both fitted linear lines do not start at the origin, however, they intersect with the Y axis at its positive side. The experimental data of 1/R vs. W, was fitted nicely ($r^2 = 0.997$, $r^2 = 0.959$ respectively) to a linear model:

$$1/R_{100nm} = A \cdot W_{1oonm} + B\ [S] \tag{2}$$

The refitting results are shown in Table 2. We can see that both parameters A and B increase as the film thickness increases.

We assume a simple model that describes the dependence of resistance in the physical properties and in the heat effected zone (HAZ). We assume that the line resistance is in parallel to the resistance of the conducive path in the HAZ:

$$\frac{1}{R} = \frac{t \cdot W}{\rho \cdot L} + \frac{t_{HAZ} \cdot W_{HAZ}}{\rho_{HAZ} \cdot L} \rightarrow A = \frac{t}{\rho \cdot L} \text{ and } B = \frac{t_{HAZ} \cdot W_{HAZ}}{\rho_{HAZ} \cdot L} \tag{3}$$

Where ρ is the PDMS/AuNP composite film resistivity. W, L, and t are the electrode's width, length, and thickness respectively. t_{HAZ}, W_{HAZ} and ρ_{HAZ} are the thickness, width and resistivity of the heat affected zone, respectively.

It can be seen that the HAZ-related parameter B increases in correlation with the film thickness. The HAZ parameter B represents the effective widening of the microelectrode's line-width due to thermal

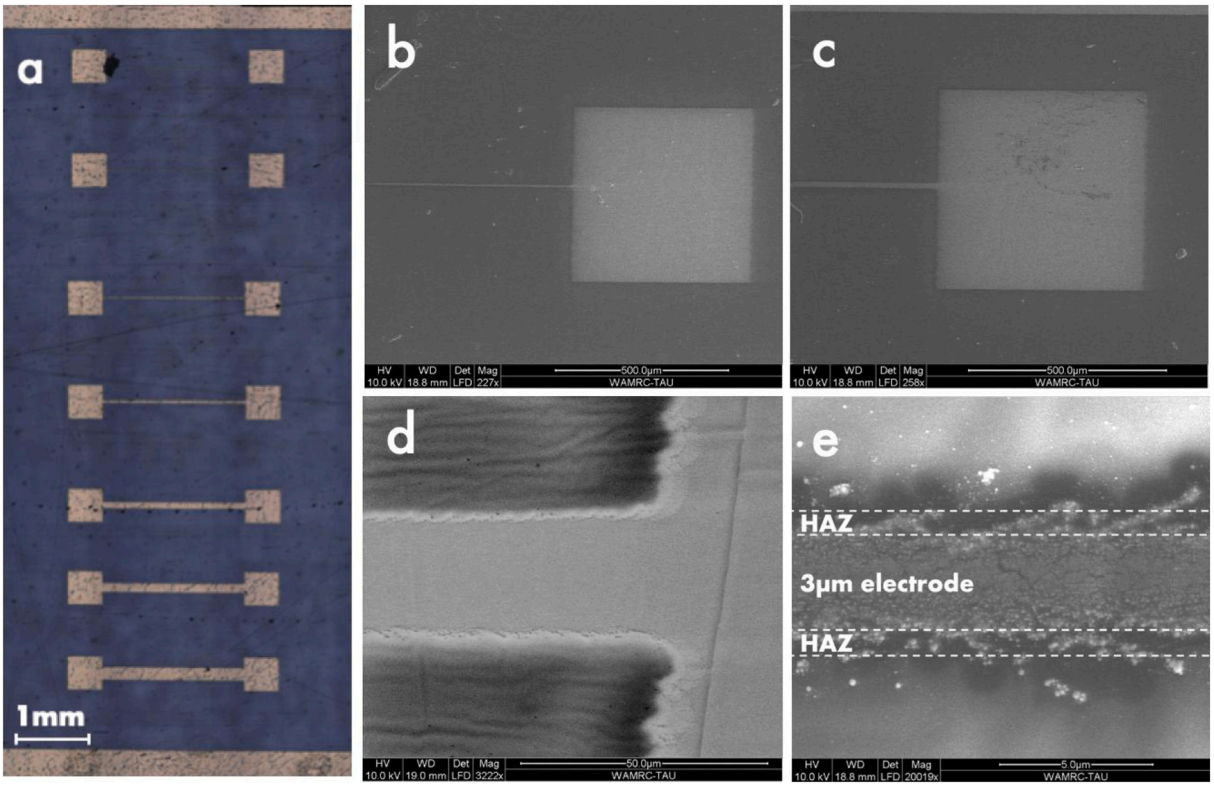


Fig. 5. The electrodes arrangement on PDMS obtained by (a) optical and (b-e) SEM imaging. The width of the electrodes in subsets (b-d) are 3 μm, 13 μm and 23 μm respectively. Figure (e) presents the electrode width and the heat affected zone.

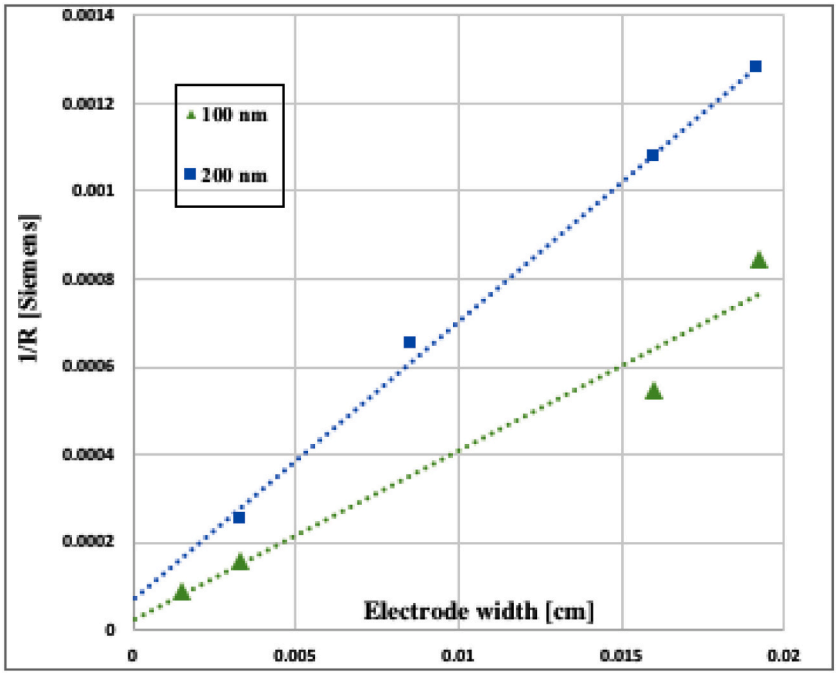


Fig. 6. Linear plot of 1/R (film resistivity) vs. the microelectrode's width for 100 nm and 200 nm equivalent thickness nanocomposite films.

effects. When assuming an ablation with a step structure, we can define the effective electrical HAZ width as B/A of eq. (3) which is proportional to the effective thickness of the film as shown in Table 2. This parameter represents the current flowing via the HAZ; thus, reducing the overall resistance. It is assumed that the increase of HAZ parameter is caused by an increase of the induced heat in the thicker film. The generated heat energy per unit area (Q') is proportional to the mass of the light absorbing gold layer that is rapidly ablated, and the mass is of course propositional to the layer's thickness: $Q' = t_{eff} \cdot c_p \cdot \triangle T$ where c_p is the heat capacitance of the gold/PDMS composite, ΔT is the temperature increase, and t_{eff} is effective thickness.

The film resistivity was extracted from each of the equations. The

Table 2
Fitting parameters of the sample conductance (1/R) to their width(W) (1/R = AxW + B).

Equivalent thickness (nm)	A (S/cm)	B (S)	Effective electrical HAZ width [μm]
100	0.0388	$2 \cdot 10^{-5}$	5.15
200	0.0637	$6 \cdot 10^{-5}$	9.42

resistivity of the 100 nm and 200 nm equivalent thickness films are $2.63e^{-3}\Omega \cdot cm$ and $2.48e^{-3}\Omega \cdot cm$ respectively, in the range of three orders of magnitude higher than bulk gold ($\rho_{gold} = 2.2e^{-6}\Omega \cdot cm$). Such higher resistivity can be explained by considering the distribution of Au clusters inside the PDMS surface. It can be concluded that the Ohmic conduction (linear I vs V) can be achieved and the gold concentration in the structure is above the percolation threshold.

4. Conclusions

In this paper we demonstrated femtosecond laser patterning of supersonic cluster beam deposited film. The deposition of gold nanoparticle onto PDMS makes supersonic cluster deposition (SCBD) one of the most suitable methods for making interconnects on flexible substrates. Currently, it is patterned using shadow mask for its patterning which limits the line width resolution to few hundred microns. In this paper, we report SCBD gold/PDMS composite patterning with lateral resolution of 3 μm.

Our results indicate that the thickness of the composite film grows in the form of $t_{actual} = k_1 \cdot t_{eq}{}^{k_2}$. Where $k_1 = 6.048$ and $k_2 = 0.759$ and the density of gold within the substrate is between 23 and 30%. The PDMS removal by ablation requires higher energy fluence than gold. It was shown that by use of a 400 mJ/cm^2, it is possible to remove the gold from the nanocomposite film without damaging the substrate. The electrodes were fabricated down to 3 μm with an effective electrical HAZ of a few micrometers, depending on the film's thickness. It was found that at a certain concentration, the film reaches a constant resistivity which is not dependent on its thickness or density. This finding allows working with relatively thin layers of a few hundred nm and still obtaining the designed resistivity. The electrical resistivity of the film was found using two different models in the range of $2.5m\Omega \cdot cm$ to $10m\Omega \cdot cm$. This resistivity is 3 orders of magnitude higher than that of bulk gold, which makes it suitable for electrodes for biosensors and various additional applications.

We conclude that the combination of SCBD and femtosecond laser processing makes them a promising technology for maskless fabrication of soft and flexible electrodes. Future work on the method includes intensive investigation and modelling of the HAZ through heat transfer mechanisms and implementation of this method in sensors fabrication.

Declaration of Competing Interest

The authors declare that they have no known competing financial interests or personal relationships that could have appeared to influence the work reported in this paper.

Acknowledgements

YS, TD and YB thank the Israel Science Foundation, Grant no. 1616/17 titled "Feasibility and Modelling of Integrated Plant Cell Functional Micro Biochip System" and the Ministry of Science and Technology, Israel, Grant # 3-14345 titled "Single-cell Sensor". We would also like to acknowledge the Boris Mints Institute for Strategic Policy Solutions to Global Challenges, the Department of Public Policy and the Manna Centre for Food Security, Tel Aviv University for their generous support under the program "Plant-based heat stress whole-cell-biosensor" (Grant no. 590351) 2017. PM, TS, LM, SMV acknowledge the financial support of Fondazione CARIPLO under project ASSIST (2018-1726), under the program 'Call to support the knowledge transfer in advanced materials research'.

Credit Author Statement.

Tali Dotan: Conceptualization, Methodology, Investigation, Writing - Original Draft.

Yuval Berg: Investigation, Writing - Original Draft.

Lorenzo Migliorini: Investigation, Writing - Original Draft.

Sara Moon Villa: Resources.

Tommaso Santaniello: Writing - Review & Editing.

Paolo Milani: Supervision, Writing - Review & Editing.

Yosi Shacham- Diamand: Supervision, Writing - Review & Editing

References

[1] M.A. McClain, I.P. Clements, R.H. Shafer, R.V. Bellamkonda, M.C. LaPlaca, M. G. Allen, Highly-compliant, microcable neuroelectrodes fabricated from thin-film gold and PDMS, Biomed. Microdevices 13 (2) (2011) 361–373.
[2] J. Kim *et al.*, "Stretchable silicon nanoribbon electronics for skin prosthesis," *Nat. Commun.*, vol. 5, 2014.
[3] N.P. Shetti, A. Mishra, S. Basu, R.J. Mascarenhas, R.R. Kakarla, T.M. Aminabhavi, Skin-Patchable Electrodes for Biosensor Applications : A Review, 2020.
[4] B.U. Hwang, et al., Transparent stretchable self-powered patchable sensor platform with ultrasensitive recognition of human activities, ACS Nano 9 (9) (2015) 8801–8810.
[5] A. Economou, C. Kokkinos, M. Prodromidis, Flexible plastic, paper and textile lab-on-a chip platforms for electrochemical biosensing, Lab Chip 18 (13) (2018) 1812–1830.
[6] K. Park, M. A. Woo, J. A. Lim, Y. R. Kim, S. W. Choi, and M. C. Lim, "In situ synthesis of directional gold nanoparticle arrays along ridge cracks of PDMS wrinkles," *Colloids Surfaces A Physicochem. Eng. Asp.*, vol. 558, no. June, pp. 186–191, 2018.
[7] D.C. Duffy, J.C. McDonald, O.J.A. Schueller, G.M. Whitesides, Rapid prototyping of microfluidic systems in poly(dimethylsiloxane), Anal. Chem. 70 (23) (Dec. 1998) 4974–4984.
[8] J. Zhou, A.V. Ellis, N.H. Voelcker, Recent developments in PDMS surface modification for microfluidic devices, Electrophoresis 31 (1) (2010) 2–16.
[9] S.P. Lacour, S. Wagner, Z. Huang, Z. Suo, Stretchable gold conductors on elastomeric substrates, Appl. Phys. Lett. 82 (15) (2003) 2404–2406.
[10] K.W. Meacham, R.J. Giuly, L. Guo, S. Hochman, S.P. DeWeerth, A lithographically-patterned, elastic multi-electrode array for surface stimulation of the spinal cord, Biomed. Microdevices 10 (2) (2008) 259–269.
[11] C. Minnai and P. Milani, "Metal-polymer nanocomposite with stable plasmonic tuning under cyclic strain conditions," *Appl. Phys. Lett.*, vol. 107, no. 7, 2015.
[12] A. Ryspayeva *et al.*, "A rapid technique for the direct metallization of PDMS substrates for flexible and stretchable electronics applications," *Microelectron. Eng.*, vol. 209, no. October 2018, pp. 35–40, 2019.
[13] T. Adrega and S. P. Lacour, "Stretchable gold conductors embedded in PDMS and patterned by photolithography: fabrication and electromechanical characterization," *J. Micromechanics Microengineering*, vol. 20, no. 5, p. 055025, May 2010.
[14] F. Borghi *et al.*, "Stretchable nanocomposite electrodes with tunable mechanical properties by supersonic cluster beam implantation in elastomers," *Appl. Phys. Lett.*, vol. 106, no. 12, 2015.
[15] S.P. Lacour, D. Chan, S. Wagner, T. Li, Z. Suo, Mechanisms of reversible stretchability of thin metal films on elastomeric substrates, Appl. Phys. Lett. 88 (20) (2006) 2004–2007.
[16] H. Stoyanov, M. Kollosche, S. Risse, R. Waché, G. Kofod, Soft conductive elastomer materials for stretchable electronics and voltage controlled artificial muscles, Adv. Mater. 25 (4) (2013) 578–583.
[17] Q. Zhang, J. Xu, Y. Liu, and H. Chen, "In-situ synthesis of poly (dimethylsiloxane)–gold nanoparticles composite films and its application in microfluidic systems {," vol. 184, pp. 352–357, 2008.
[18] M.G. Urdaneta, R. Delille, E. Smela, Stretchable electrodes with high conductivity and photo-patternability, Adv. Mater. 19 (18) (2007) 2629–2633.
[19] I. Byun, A. W. Coleman, and B. Kim, "Transfer of thin Au films to polydimethylsiloxane (PDMS) with reliable bonding using (3-mercaptopropyl) trimethoxysilane (MPTMS) as a molecular adhesive," *J. Micromechanics Microengineering*, vol. 23, no. 8, 2013.
[20] R. Seghir and S. Arscott, "Controlled mud-crack patterning and self-organized cracking of polydimethylsiloxane elastomer surfaces," *Sci. Rep.*, vol. 5, no. March, pp. 1–16, 2015.
[21] O. Akogwu, D. Kwabi, S. Midturi, M. Eleruja, B. Babatope, W.O. Soboyejo, Large strain deformation and cracking of nano-scale gold films on PDMS substrate, Mater. Sci. Eng. B Solid-State Mater. Adv. Technol. 170 (1–3) (Jun. 2010) 32–40.
[22] T. Baëtens, E. Pallecchi, V. Thomy, S. Arscott, Cracking effects in squashable and stretchable thin metal films on PDMS for flexible microsystems and electronics, Sci. Rep. 8 (1) (2018) 1–17.

[23] T. Adrega and S. P. Lacour, "Stretchable gold conductors embedded in PDMS and patterned by photolithography: Fabrication and electromechanical characterization," *J. Micromechanics Microengineering*, vol. 20, no. 5, 2010.
[24] I. Turjeman, T. Dotan, Y. Berg, Z. Kotler, D. Sherman, Y. Shacham-Diamand, Mechanical Modeling of Metal Thin Films on Elastomers for Femtosecond Laser Patterned Interconnects, Submitt. to JMEE, July, 2020.
[25] S.P. Lacour, D. Chan, S. Wagner, T. Li, Z. Suo, Mechanisms of reversible stretchability of thin metal films on elastomeric substrates, Appl. Phys. Lett. 88 (20) (2006) 2004–2007.
[26] L. Ravagnan, G. Divitini, S. Rebasti, M. Marelli, P. Piseri, and P. Milani, "Poly (methyl methacrylate)-palladium clusters nanocomposite formation by supersonic cluster beam deposition: A method for microstructured metallization of polymer surfaces," *J. Phys. D. Appl. Phys.*, vol. 42, no. 8, 2009.
[27] M. Marelli *et al.*, "Flexible and biocompatible microelectrode arrays fabricated by supersonic cluster beam deposition on SU-8," *J. Micromechanics Microengineering*, vol. 21, no. 4, 2011.
[28] A. Bellacicca, C. Prof, and F. Ragusa, "Smart materials for stretchable electronics, sensors and soft actuation," 2016.
[29] C. Ghisleri *et al.*, "Patterning of gold-polydimethylsiloxane (Au-PDMS) nanocomposites by supersonic cluster beam implantation," *J. Phys. D. Appl. Phys.*, vol. 47, no. 1, 2014.
[30] 6 John A. Rogers1 Dae-Hyeong Kim, 1* Jong-Hyun Ahn, 2* Won Mook Choi, 1* Hoon-Sik Kim, 1 Tae-Ho Kim, 1 Jizhou Song, 3 Yonggang Y. Huang, 5† Zhuangjian Liu, 6 Chun Lu, "stretch force reduction due to nanotube meander- ing. This structure provides a volume per strut of D`L 2 sin(120°) and a calculated density of r," *Nature*, vol. 320, no. April, pp. 507–511, 2008.
[31] Y. Berg, S. Winter, Z. Kotler, Y. Shacham-Diamand, Embedded metal microstructures in glass substrates by a combined laser trenching and printing process, J. Laser Micro Nanoeng. 13 (2) (2018) 131–134.
[32] Y. Berg, M. Zenou, O. Dolev, and Z. Kotler, "Temporal pulse shaping for smoothing of printed metal surfaces," *Opt. Eng.*, vol. 54, no. 1, p. 011010, 2015.
[33] M. Zenou, Z. Kotler, Printing of metallic 3D micro-objects by laser induced forward transfer, Opt. Express 24 (2) (2016) 1431–1446.
[34] M. Zenou, A. Sa'ar, and Z. Kotler, "Digital laser printing of aluminum micro-structure on thermally sensitive substrates," *J. Phys. D. Appl. Phys.*, vol. 48, no. 20, p. 205303, 2015.
[35] J.K. Chen, J.E. Beraun, Modelling of ultrashort laser ablation of gold films in vacuum, J. Opt. A Pure Appl. Opt. 5 (3) (2003) 168–173.
[36] C. Von Der Heide, M. Grein, G. Bräuer, and A. Dietzel, "Methodology of selective metallic thin film ablation from susceptible polymer substrate using pulsed femtosecond laser," *eprint arXiv:2002.00752*, pp. 1–11, 2020.
[37] J.F. Duesing, O. Suttmann, J. Koch, U. Stute, L. Overmeyer, Ultrafast laser patterning of thin films on 3-D shaped surfaces for strain sensor applications, J. Laser Micro Nanoeng. 7 (3) (2012) 311–315.
[38] S. Amoruso, N.N. Nedyalkov, X. Wang, G. Ausanio, R. Bruzzese, P.A. Atanasov, Erratum: ultrashort-pulse laser ablation of gold thin film targets: theory and experiment (thin solid films (2014) 550 190-198), Thin Solid Films 551 (2014) 205.
[39] E. Mishuk *et al.*, "Femtosecond laser processing of ceria-based micro actuators," *Microelectron. Eng.*, vol. 217, no. March, p. 111126, 2019.
[40] K. Wegner, P. Piseri, H. V. Tafreshi, and P. Milani, "Cluster beam deposition: A tool for nanoscale science and technology," *J. Phys. D. Appl. Phys.*, vol. 39, no. 22, 2006.
[41] I. D. Johnston, D. K. McCluskey, C. K. L. Tan, and M. C. Tracey, "Mechanical characterization of bulk Sylgard 184 for microfluidics and microengineering," *J. Micromechanics Microengineering*, vol. 24, no. 3, 2014.
[42] S. Preuss, A. Demchuk, M. Stuke, Sub-picosecond UV laser ablation of metals, Appl. Phys. A Mater. Sci. Process. 61 (1) (1995) 33–37.
[43] J.K. Chen, J.E. Beraun, Modelling of ultrashort laser ablation of gold films in vacuum, J. Opt. A Pure Appl. Opt. 5 (3) (2003) 168–173.
[44] H. Huang and Z. Guo, "Ultra-short pulsed laser PDMS thin-layer separation and micro-fabrication," *J. Micromechanics Microengineering*, vol. 19, no. 5, 2009.
[45] S.H. Ko, Y. Choi, D.J. Hwang, C.P. Grigoropoulos, J. Chung, D. Poulikakos, Nanosecond laser ablation of gold nanoparticle films, Appl. Phys. Lett. 89 (14) (2006) 2004–2007.
[46] O. Suttmann, J. Duesing, and L. Overmeyer, "Phenomenological model for prediction of complex ablation geometries in metal films using ultrashort laser pulses," *J. Laser Appl.*, vol. 28, no. 2, p. 022208, 2016.
[47] J.G. Simmons, Generalized formula for the electric tunnel effect between similar electrodes separated by a thin insulating film, J. Appl. Phys. 34 (6) (1963) 1793–1803.